A canopy radiative transfer scheme with explicit FAPAR for the interactive vegetation model ISBA-A-gs: Impact on carbon fluxes

Dominique Carrer, Jean-Louis Roujean, Sebastien Lafont, Jean-Christophe Calvet, Aaron Boone, Bertrand Decharme, Christine Delire, Jean-Philippe Gastellu-Etchegorry

JOURNAL OF GEOPHYSICAL RESEARCH: BIOGEOSCIENCES, VOL. 118, 888–903, doi:10.1002/jgrg.20070, 2013

A canopy radiative transfer scheme with explicit FAPAR for the interactive vegetation model ISBA-A-gs: Impact on carbon fluxes

Dominique Carrer,[1] Jean-Louis Roujean,[1] Sébastien Lafont,[1] Jean-Christophe Calvet,[1] Aaron Boone,[1] Bertrand Decharme,[1] Christine Delire,[1] and Jean-Philippe Gastellu-Etchegorry[2]

Received 20 August 2012; revised 6 May 2013; accepted 11 May 2013; published 17 June 2013.

[1] Vegetation attributes impact the Earth's carbon, water, and energy budgets by controlling the exchanges between the lower atmosphere and the continental biosphere. One of the most important factors is the distribution of the absorbed fraction of solar radiation within vegetation as it constrains the photosynthesis rate. The Interactions Surface-Biosphere-Atmosphere, CO_2-responsive (ISBA-A-gs) interactive vegetation model developed at Meteo-France is particularly well designed to simulate the vegetation fluxes. A new radiation transfer scheme for the canopy has been designed and implemented in ISBA-A-gs, which adopts a self-shading approach. This means that the incoming solar fluxes at the top of the canopy will hit a number of canopy layers prior to reaching the soil background. The photosynthesis model calculates the net assimilation of CO_2 of each canopy layer using the absorbed photosynthetically active radiation (PAR) flux of the layer. Integration is carried out to obtain a quantitative estimate of the total net assimilation for the whole canopy layer by summing the contribution of each canopy sublayer. Assessment of the vegetation transmittance and canopy light response is then performed. Quantitative estimates of the impact on gross primary production (GPP) in local stations are presented. Also, global estimates of the fraction of absorbed PAR modeled with ISBA-A-gs are shown. This study demonstrates the added value of the upgraded canopy radiation transfer model for the simulation of GPP.

Citation: Carrer, D., J.-L. Roujean, S. Lafont, J.-C. Calvet, A. Boone, B. Decharme, C. Delire, and J.-P. Gastellu-Etchegorry (2013), A canopy radiative transfer scheme with explicit FAPAR for the interactive vegetation model ISBA-A-gs: Impact on carbon fluxes, *J. Geophys. Res. Biogeosci.*, *118*, 888–903, doi:10.1002/jgrg.20070.

1. Introduction

[2] Vegetation surfaces play a key role in the Earth's energy balance and have a major impact on the global carbon cycle. For instance, photosynthesis is responsible for the conversion of about 50 PgC yr^{-1} of atmospheric CO_2 into biomass, which represents about 10% of the atmospheric carbon. Current estimates suggest that land use changes lead to the emission of 1.7 PgC yr^{-1} in the tropics [*Laurila*, 2002], mainly due to deforestation, and to a small amount of uptake (about 0.1 PgC) in temperate and boreal areas—thereby producing a net source of around 1.6 PgC yr^{-1} [*Houghton*, 1995]. Despite the fact that these aforementioned numbers exist, the distribution by latitude of carbon sources and sinks remains a core question, being matter of debate for a broad scientific community. In this regard, a better representation of vegetation processes in the ecological modeling is desirable.

[3] The fraction of solar radiation that is absorbed by a vegetation canopy constrains the rate of photosynthesis and the amount of carbon flux either fixed or released to the atmosphere by this same canopy layer. Radiation absorption is inferred from the knowledge of the characteristics of a collimated radiation beam impinging on the surface, which is then scattered in several directions. Clearly, such phenomenon results from complex nonlinear radiation transfer processes determining the amount of radiation that is transmitted through the vegetation. The radiation regime depends primarily on the structural properties of the vegetation, i.e., the leaf orientation and distribution, the leaf area density, the gap size within the canopy, the crown or plant stand shape. Also, the physiology of the leaves associated with the magnitude of the single-scattering albedo determines how much light a single leaf ingests after it was hit by a series of photons. This depends on the growing stage of the vegetation and can be formulated in terms

[1]Centre National de Recherches Météorologiques-GAME, UMR3589, Centre National de la Recherche Scientifique, Météo-France, Toulouse, France.
[2]Centre d'Etudes Spatiales de la Biosphere, Toulouse, France.

Corresponding author: D. Carrer, Centre National de Recherches Météorologiques-GAME, UMR3589, Centre National de la Recherche Scientifique, 42, Météo-France, Ave. Gaspard Coriolis, FR-31057 Toulouse CEDEX, France. (dominique.carrer@meteo.fr)

2169-8953/13/10.1002/jgrg.20070

of wavelength dependence. The partitioning of solar radiation between diffuse and direct components is crucial because diffuse conditions let more sunlight strike the inner part of the canopy. As a result, this means more light absorption by the entire canopy. However, days with high diffuse radiation are cloudy days, associated with less thermal stress on plants. The component of diffuse radiation within the canopy is a blended contribution from the atmospheric particles (clouds, aerosols) and leaf scatters, the latter depending on the structural organization of the vegetation canopy and on the spectral properties of the leaves. It was established that the prescription of a diffuse radiation component is critical for properly capturing the photosynthesis rate of plant stands [*Mercado et al*., 2009].

[4] The process of carbon assimilation by vegetation is driven by the atmospheric CO_2 concentration, the characteristics of incident photosynthetically active radiation (PAR), the photosynthetic capacity of the leaves, and also some other factors that control the distribution of solar radiation over the leaves [*DeWit*, 1965; *Jarvis*, 1976]. The CO_2 fluxes exchanged between the surface and the atmosphere are closely linked to the surface energy and water budgets of the surface. For this reason and bearing in mind that the atmospheric CO_2 concentration influences the canopy conductance [*Calvet et al*., 2008; *Ceulemans and Mousseau*, 1994; *Fitter and Hay*, 2002; *Schlesinger*, 1997, and references therein], soil vegetation atmosphere transfer (SVAT) models used in climate and weather prediction models are by necessity becoming increasingly complex [e.g., *Dai et al*., 2003; *Sellers et al*., 1996].

[5] It is worthwhile to mention here the lessons learned from the RAMI4PILPS initiative, which consists in an intercomparison of various radiative transfer (RT) codes in order to give rise to meaningful approaches [*Widlowski et al*., 2011]. One of the main outcomes of this intercomparison effort is that both simplified and detailed 3D modeling closely satisfies the criterion of energy conservation for homogeneous canopies having uniform foliage orientation. This satisfactory model-to-model agreement generally deteriorates as the plant canopy contains a more complex structure [*Duthoît et al*., 2008; *Widlowski et al*., 2011]. For a given canopy, the largest deviations occur for the simulated canopy absorption and transmission terms in diffuse illumination conditions. However, the necessity for including complex 3D RT codes into SVAT models devoted to global scale studies still appears questionable as the exact structure of the canopy is not explicitly known [e.g., *Ni-Meister and Gao*, 2011]. These outcomes seem to be in favor of a pragmatic approach for which future SVAT models will incorporate RT codes simple to calibrate in trading accuracy for speed.

[6] The RT code within the canopy of the ISBA-A-gs (Interactions Surface-Biosphere-Atmosphere, CO_2-responsive) land surface model (LSM) was defined according to a self-shading approach [*Calvet et al*., 1998]. Both expressions of direct and diffuse terms of transmittance corresponded to a random canopy and were available from visible until midinfrared radiation [*Roujean*, 1996]. Originally, a relatively low atmospheric turbidity was prescribed, and the diffuse fraction had no dependence on the cloudiness. At each level of the canopy, attenuated PAR was computed and a photosynthesis model derived from *Jacobs* [1994] served to estimate the leaf net assimilation *(An)*. Furthermore, integration was performed in order to obtain an average quantity for the entire vegetation canopy. The complex nonlinear photosynthesis response of the exposed leaves justified such an approach in the original version of ISBA-A-gs. Gaussian quadrature weights were fixing the contribution of each canopy sublayer [*Goudriaan*, 1986]. Consequently, this way of handling modeled canopy photosynthesis did not necessarily match the corresponding PAR absorption for the whole canopy. A detailed description of the original vegetation RT scheme within the canopy can be found in Appendix B of *Calvet et al*. [1998].

[7] The objective of the present study is to yield coherent improvements in the ISBA-A-gs radiative modeling along several directions and to evaluate their impact on photosynthesis. In this respect, this work resembles a recent study conducted with the Community Land Model version 4 (CLM4) [e.g., *Bonan et al*., 2011] aimed at investigating the use of a better description of the radiation beam within the canopy to reduce the substantial overestimation of carbon uptake of CLM4 at the global scale. The results from a multilayer canopy model on the photosynthesis module are considered because it prevails in the estimates of gross primary production (GPP). Moreover, this paper presents a proof-of-concept for the Land Surface Model (LSM) simulation of the fraction of absorbed PAR (FAPAR), which could have many applications for LSM benchmarking and in the field of assimilation of satellite-derived products in upcoming years.

[8] The present manuscript is organized as follows: section 2 presents the coupling between the ISBA-A-gs photosynthesis module and a new multilayer vegetation RT model. This latter will be referred hereafter as NEW, whereas the reference version of the RT module used hitherto in ISBA-A-gs will be named REF. The experimental designs for the different simulations are detailed in this same section. Vegetation transmittance functions and various canopy light-response curves of the new multilayer canopy model are assessed in section 3, which also contains a presentation of annual estimates of globally modeled FAPAR with ISBA-A-gs. Evaluation of GPP at the global scale with the ISBA-A-gs model is shown for the first time. Section 4 discusses these results according to previous related studies. This points out the value-added brought by the use of a multilayer vegetation radiative transfer model for GPP modeling and the outcomes issued from a diagnostic analysis of the variable FAPAR. Section 5 summarizes and concludes the study in stressing its future perspectives.

2. Materials and Methods

2.1. Radiative Transfer Model

[9] This section is devoted to the presentation of a vegetation canopy embedded in a multislice model for the purpose of its implementation in the RT scheme of the ISBA-A-gs model. Light diffusion of solar radiation within a vegetation canopy is the outcome of complex interactions of a group of photons traveling deeply in the whole foliage slab bypassing through it or hitting phytoelements. The bottom part is bounded by the soil background, which forms a semireflective and impervious surface. The outputs of such vegetative systems depend merely on four ingredients [e.g., *Ross*, 1981]: (i) the architecture of individual plants and the canopy shape; (ii) the optical properties of phytoelements; (iii) the reflective properties of the ground underneath the canopy, and (iv) the atmospheric conditions.

These element properties can be well depicted using the RT theory. In order to mimic the vertical heterogeneity of vegetation canopies (e.g., the forest crown versus trunk layers), two sets of canopy parameters are used, one for the top layer and one for the bottom layer. Our portrait of the canopy is applicable for any vegetation type, inclusive low vegetation, as far significant vertical profiles of leaf density and properties are present [*Lantinga et al*., 1999]. Each stratum is sliced into several layers of leafy material. The calculation of the associated vegetation transmittance functions is detailed here below.

2.1.1. Vertical Grid Within Canopy

[10] Theoretical studies [*Ni et al*., 1997] and also ground measurements [*Roujean*, 1999] led to the conclusion that the relative proportion of light transmittance decreases from top to bottom of the canopy in a nonlinear fashion with sharpest variations obtained at the top of the canopy. Hence, the definition of the vertical grid for the vegetation canopy should be thinner at the top than at the bottom. By adopting a Gauss vertical profile [e.g., *Goudriaan*, 1986], the grid definitions for 10 levels in normalized height units are 0.99, 0.93, 0.84, 0.72, 0.57, 0.43, 0.28, 0.16, 0.07, and 0.00.

2.1.2. Diffuse Fraction

[11] The ratio between diffuse and direct radiation is a fundamental attribute. At least for the top of canopy, it depends to a large extent on the atmospheric compounds (aerosols and clouds). Note that the angular distribution of the leaves is a less essential variable when diffuse radiation is prominent. As a matter of fact, larger diffuse component enhances the light distribution within the canopy and increases the assimilation rate [*Goudriaan*, 1977]. In this study, the diffuse radiation at a given canopy level is the sum of the incoming atmospheric diffuse component ($\mathrm{fd_{sky}}$) and the diffuse radiation arising from multiple-scattering interactions at each canopy sublayer ($\mathrm{fd_{veg}}$). The influence of the atmosphere is obviously lesser for a sublayer approaching the soil background.

[12] The initial value of the diffuse fraction is driven by a clearness index, *Kt*, which shows a decay with the cloudiness [*Erbs et al*., 1982]. Under clear-sky conditions, the estimation of diffuse fraction is slightly different from *Erbs et al*. [1982], which suggested a constant value of 0.165. Instead, we stipulate here that the diffuse fraction will only depend on the aerosol optical depth. This latter was arbitrarily fixed here to 0.1 in order to enhance the impact of diffuse light on the photosynthesis in the presence of a standard atmosphere with a low aerosol burden. The clearness index is defined as:

$$\mathrm{Kt} = \mathrm{Rg}/(C_s \mu_s) \tag{1}$$

for $Kt \le 0.22$, $\mathrm{fd_{sky}} = 1 - 0.09\mathrm{Kt}$,

$$0.22 < \mathrm{Kt} < 0.8,\ \mathrm{fd_{sky}} = 0.9511 + (-0.1604 + (4.388 + (-16.64 + 12.34 \times \mathrm{Kt})\mathrm{Kt})\mathrm{Kt})\mathrm{Kt},$$

$Kt \ge 0.8$, $\mathrm{fd_{sky}} = (1 - \exp(-\tau))/(1 - (1 - \mu s)\exp(-\tau))$,

where μ_s is the cosine of the solar zenith angle, C_s is the solar constant assumed to be equal to 1368 W/m^2, Rg is the global solar radiation, and τ is the aerosol optical depth.

[13] Once the radiation beam has entered the canopy, the multiple-scattering component becomes a fast-growing function of the foliage mass iteratively supplied by the different sublayers. This can be formulated by introducing an elementary leaf slab positioned at a depth x from the top. The corresponding optical thickness is $(1 - x)$ leaf area index (LAI), with LAI being the ratio "Leaf area" per "Horizontal ground area." After it was crossed by the direct part of light, the resulting diffuse fraction will read:

$$\mathrm{fd_{veg}}(x) = \frac{1 - \exp^{-\Omega_{\mathrm{dr}}^{\mathrm{sup}} \mathrm{LAI}(1-x)}}{1 - (1 - \mu_s)\exp^{-\Omega_{\mathrm{dr}}^{\mathrm{sup}} \mathrm{LAI}(1-x)}} \tag{2}$$

where Ω is the clumping index, a quantity to be developed in the next section.

[14] Consequently, the total diffuse fraction fd of the light reaching the layer below the depth x reads:

$$\mathrm{fd} = \min\left[1; \left(\mathrm{fd_{sky}} + \mathrm{fd_{veg}}\right)\right] \tag{3}$$

2.1.3. Clumping Index

[15] Ω represents the level of aggregation of the phytoelements within the canopy. It is an intrinsic property of a canopy that may vary under environmental stress factors and with plant growth. It is also expected to vary along a vertical profile within the canopy. In this work, Ω yields a distinct parameterization for the direct ("dr") and diffuse ("df") radiation components. Two different parameterizations of Ω are used to depict the light efficiency, which will have different impact if the considered leaf layer belongs to the top ("sup") or bottom ("inf") part of the canopy. Viz:

$$\begin{aligned} \Omega_{\mathrm{dr}}^{\mathrm{sup/inf}} &= \frac{1}{1 + \sigma_{\mathrm{sup/inf}} \exp^{-k_{\mathrm{sup/inf}}(\cos^{-1}(\mu_s))^{d\,\mathrm{sup/inf}}}} \\ \Omega_{\mathrm{df}}^{\mathrm{sup/inf}} &= \frac{1 + 0.5 \times \sigma_{\mathrm{sup/inf}}}{1 + \sigma_{\mathrm{sup/inf}}} \end{aligned} \tag{4}$$

where μ_s is the cosine of the solar zenithal angle, and $\sigma_{\mathrm{sup/inf}}$, $k_{\mathrm{sup/inf}}$, $d_{\mathrm{sup/inf}}$ are coefficients that are expressed as a function of the geometry of the crown and the ratio between the height and the diameter of the crown [*Kucharik et al*., 1999] (Table 1). Note that *Kucharik et al*. [1999] obtained a calibration of equation (4) based on Monte Carlo simulations.

2.1.4. Completion of Transmittance Function

[16] Finally, all parameterizations contribute to the definition of direct and diffuse transmittance functions that allow a thorough examination of the impact of the radiation regime for the entire vegetation canopy.

[17] At this stage, distinct formulations for direct and diffuse transmittance function are to be defined. The light path within the canopy is sliced in N elementary foliage slabs characterized by their thickness Δx. At a level indexed i, the two transmittance factors will read:

$$\begin{aligned} T_{\mathrm{dr}}^{\mathrm{sup/inf}}(\Delta x_i) &= \exp\left(-g_{\mathrm{sup/inf}} b_{\mathrm{dr}}^{\mathrm{sup/inf}} \Omega_{\mathrm{dr}}^{\mathrm{sup/inf}} LAI\ \Delta x_i/\mu_s\right) \\ T_{\mathrm{df}}^{\mathrm{sup/inf}}(\Delta x_i) &= \exp\left(-b_{\mathrm{df}}^{\mathrm{sup/inf}} \Omega_{\mathrm{df}}^{\mathrm{sup/inf}} LAI\ \Delta x_i\right) \end{aligned} \tag{5}$$

where b is the foliage-scattering coefficient [*Roujean*, 1996] of the layer (Table 1), and g is the ratio "leaf cross section, per leaf area." The latter depends on the incident direction and on the leaf angle distribution. Various model distribution functions for leaf normal inclination were proposed by *DeWit*

Table 1. Values of the Coefficients Used in the Calculation of the Transmittance Function in the PAR Spectrum[a]

Coefficients of the Transmittance Function	
$b_{\mathrm{dr}}^{\mathrm{sup/inf}}$	$1-\frac{1-\sqrt{1-\mathrm{SSA}_{\mathrm{sup/inf}}}}{1+2\mu_s\sqrt{1-\mathrm{SSA}_{\mathrm{sup/inf}}}}$ where SSA is the single-scattering albedo of the leaf of the layer. Arbitrary fixed to 0.15 in the PAR domain
$b_{\mathrm{df}}^{\mathrm{sup/inf}}$	$1-\frac{1-\sqrt{1-\mathrm{SSA}_{\mathrm{sup/inf}}}}{1+\sqrt{1-\mathrm{SSA}_{\mathrm{sup/inf}}}}$ where SSA is the single-scattering albedo of the leaf of the layer. Arbitrary fixed to 0.15 in the PAR domain
g_{sup} and g_{inf}	0.5 value characterizing spherical distribution of leaves is used.
k_{sup} and k_{inf}	2.tan(zc)with zc = 50° angle of inclination of the crown1 value is used.
σ_{sup} and σ_{inf}	$\frac{\Omega_{\max}-\Omega(\theta)}{\Omega(\theta)\exp\left(-k(\theta)^d\right)}$ where values of $\Omega_{\max}$ and $\Omega(\theta=0)$ potentially permit to derive this σ coefficient.Values between 1 (crop type) and 4 (forest type) are used.
d_{sup}	$-0.461.\chi_{\mathrm{sup}}+3.8$ with $\chi_{\mathrm{sup}}=2.$ ratio between height and diameter of the crown
d_{inf}	$-0.461.\chi_{\mathrm{inf}}+3.8$ with $\chi_{\mathrm{inf}}=7.$ ratio between height and diameter of the crown

[a]A detailed description of the equations is given in *Kucharik et al*. [1999].

[1965] and *Bunnik* [1978] for mostly horizontal leaves (planophile), mostly erectophile leaves (erectophile), mostly leaves at 45° (plagiophile), mostly horizontal and vertical leaves (extremophile), or for all possible inclinations (uniform). We opted for a uniform distribution, as it appears appropriate for satellite applications from moderate to coarse scale resolution where randomness is probably prevalent. For this leaf angle distribution, g does not depend on the incident light direction.

[18] Accounting for the diffuse fraction seems particularly relevant for vegetation functional models. The diffuse illumination tends to amplify the photosynthesis due to an enhanced efficiency of light absorption since more leaves will be hit by photons in this case. The transmittance at depth i could be derived as being equal to the product of the transmittance of each depth l of thickness $\Delta x_l = x(l) - x(l-1)$ from the top of the canopy to the attained depth i:

$$T_i = \prod_{l=1}^{i}\left[(1-\mathrm{fd}(x_{l-1}))T_{\mathrm{dr}}^{\mathrm{sup/inf}}(\Delta x_l) + \mathrm{fd}(x_{l-1})T_{\mathrm{df}}^{\mathrm{sup/inf}}(\Delta x_l)\right) \quad (6)$$

2.2. Photosynthesis Integration

[19] Light absorption by the photosynthetic pigments shows peaks mostly in the blue and in the red spectral bands, which are located at the extreme positions of the PAR range [400–700 nm]. The energy contained in the PAR represents about half the solar energy (*Rg*) received at the Earth's surface [*Ross*, 1975; *Goudriaan*, 1977]. The coupling between the photosynthesis module and the NEW multilayer vegetation RT model is detailed hereafter.

2.2.1. Vegetation Radiative Transfer Modeling

[20] The absorbed PAR radiation (aPAR) from the top of the canopy to the depth i (N being the lowermost canopy level) reads:

$$\begin{aligned}
&\text{if } i \neq N \quad \mathrm{aPAR}_i = \left(1-\alpha_{\mathrm{veg}}\right)(1-T_i)\ 0.48\mathrm{Rg}\\
&\text{if } i = N \quad \mathrm{aPAR}_{i=N} = \left(1-\alpha_{\mathrm{veg}}\right)(1-T_{i=N})\ 0.48\mathrm{Rg}\\
&\qquad\qquad +\alpha_{\mathrm{soil}}\left(1\text{-}\alpha_{\mathrm{veg}}\right)^2(1\text{-}T_{\mathrm{df}})\ T_{\mathrm{i}=N}\times 0.48\mathrm{Rg} \quad (7)
\end{aligned}$$

where α_{veg} and α_{soil} stand for the vegetation albedo and bare soil albedo, respectively. The value of 0.48 adopted here represents a widespread value of PAR/Rg at midlatitudes. It must be noted that *McCree* [1966] and *Stigter and Musabilha* [1982] reported that PAR/Rg can be greater than 0.6 under very cloudy skies. Similarly, *Tsubo and Walker* [2005] showed that PAR/Rg tends to increase as the clearness index (Kt) decreases. T_{df} is the diffuse transmittance corresponding to the upward radiation flux from the surface to the top of the canopy.

2.2.2. Sunlit/Shaded Leaves

[21] At a given a level within the canopy, all the leaves do not necessarily absorb the same amount of light. Considering the existence of sunlit leaves and shaded leaves, then the photosynthesis rate by leaves is a nonlinear function [*Duncan et al*., 1967]. Hence, the fractions of aPAR absorbed by the sunlit and shaded leaves, $\mathrm{aPAR}_{\mathrm{sunlit}}$ and $\mathrm{aPAR}_{\mathrm{shade}}$, respectively, must be distinguished [e.g., *Dufrêne et al*., 2005]:

$$\begin{aligned}
\mathrm{aPAR}_{\mathrm{sunlit}}^{i} &= \frac{(1-\mathrm{fd})\ \Delta\mathrm{aPAR}_i}{\Delta\mathrm{LAI}_i.p_{\mathrm{sun}}} + \frac{\mathrm{fd}\ \Delta\mathrm{aPAR}_i}{\Delta\mathrm{LAI}_i}\\
aPAR_{shade}^{i} &= \frac{\mathrm{fd}\Delta\ \mathrm{aPAR}_i}{\Delta\mathrm{LAI}_i}
\end{aligned} \quad (8)$$

with $\Delta\mathrm{aPAR}_i = \mathrm{aPAR}(x_i) - \mathrm{aPAR}(x_{i-1})$, $\Delta\mathrm{LAI}_i = \Delta x_i \times \mathrm{LAI}$, and p_{sun} is the mean proportion of sunlit leaves in layer i. *Dufrêne et al*. [2005] suggest to approximate p_{sun} by the total transmittance T at layer i (total means from the top to the layer i). The values of $\mathrm{aPAR}_{\mathrm{sunlit}}$ and $\mathrm{aPAR}_{\mathrm{shade}}$ are the correct quantities for light to be used by the photosynthesis model. Finally, the daily modeled FAPAR is computed from the instantaneous ISBA-A-gs estimates as:

$$\mathrm{FAPAR} = \sum\left[\mu_s x(\mathrm{aPAR}_{\mathrm{shade}} + \mathrm{aPAR}_{\mathrm{sunlit}})\right] / \sum\left[\mu_s x 0.48\mathrm{Rg}\right] \quad (9)$$

2.2.3. Leaf Net Assimilation

[22] Photosynthesis models are based on ecophysiology studies and described the properties of a single leaf. We use here the photosynthesis model of Jacobs based on the approach proposed by *Goudriaan et al*. [1985]. The integration of a photosynthesis model from leaf to canopy scale is not straightforward. This is why we will try to describe "mean leaves" that are representative of each canopy level (described in section 2.1).

[23] In order to assess the net assimilation resulting from an idealized leaf representative of a given layer of the canopy, we consider N layers of leaves mimicking the N levels. The N values of absorbed PAR are then estimated for sunlit and shaded leaves, that is $\mathrm{aPAR}_{\mathrm{sunlit}}$ and $\mathrm{aPAR}_{\mathrm{shade}}$,

Table 2. List of the 37 FLUXNET Local Stations of Conifer ("Coni"), Deciduous ("Deci"), and Tropical Forest ("Trop")

Station	Latitude	Longitude	Biome
AU-Tum	−35.66	148.15	Trop.
AU-Wac	−37.43	145.19	Trop.
BR-Sa3	−3.02	−54.97	Trop.
CA-Man	55.88	−98.48	Coni.
CA-NS1	55.88	−98.48	Coni.
CA-NS2	55.91	−98.52	Coni.
CA-NS3	55.91	−98.38	Coni.
CA-NS4	55.91	−98.38	Coni.
CA-NS5	55.86	−98.49	Coni.
CA-Qcu	49.27	−74.04	Coni.
CA-Qfo	49.69	−74.34	Coni.
CA-SF1	54.49	−105.82	Coni.
CA-SF2	54.25	−105.88	Coni.
DE-Tha	50.96	13.57	Coni.
FI-Hyy	61.85	24.29	Coni.
ID-Pag	2.35	114.04	Trop.
IL-Yat	31.34	35.05	Coni.
IT-Cpz	41.71	12.38	Trop.
IT-Ro1	42.41	11.93	Deci.
IT-Ro2	42.39	11.92	Deci.
NL-Loo	52.17	5.74	Coni.
SE-Fla	64.11	19.46	Coni.
SE-Nor	60.09	17.48	Coni.
SE-Sk2	60.13	17.84	Coni.
US-Bar	44.06	−71.29	Deci.
US-Blo	38.90	−120.63	Coni.
US-Ha1	42.54	−72.17	Deci.
US-Ho1	45.20	−68.74	Coni.
US-Ho2	45.21	−68.75	Coni.
US-Me4	44.50	−121.62	Coni.
US-MMS	39.32	−86.41	Deci.
US-PFa	45.95	−90.27	Deci.
US-Syv	46.24	−89.35	Deci.
US-UMB	45.56	−84.71	Deci.
US-WBW	35.96	−84.29	Deci.
US-WCr	45.81	−90.08	Deci.
Hesse	48.67	7.06	Deci.

respectively. These N levels within the canopy serve to formulate N average equivalent leaves having N different absorbed radiation properties. A transposition of the net assimilation from a single leaf and given level to the entire canopy has to be performed. For a given layer i, the leaf net assimilations of sunlit (An^i_{sunlit}) and shaded (An^i_{shade}) leaves are calculated through the use of the asymptotic exponential light response function [*Goudriaan et al*., 1985]:

$$\begin{aligned} An^i_{sunlit} &= (Am + Rd)\left(1 - \exp\left(\frac{-\varepsilon \times aPAR^i_{sunlit}}{Am + Rd}\right)\right) - Rd \\ An^i_{shade} &= (Am + Rd)\left(1 - \exp\left(\frac{-\varepsilon \times aPAR^i_{shade}}{Am + Rd}\right)\right) - Rd \end{aligned} \quad (10)$$

where Rd is the leaf respiration, Am is the maximum net assimilation, and ε denotes the initial quantum use efficiency, quantifying the slope of the light response curve. Finally, the average leaf net assimilation (An) representative of the entire canopy is assessed after multiplying by the thickness of the layer:

$$A_n = \sum_{i=1}^{N}\left[p_{sun}A^i_{n\ sunlit} + (1 - p_{sun})A^i_{n\ shade}\right]\Delta x_i \quad (11)$$

[24] Further, the canopy net assimilation will become $A_c = A_n . LAI$ after an integration over the whole canopy layer. Note that a similar upscaling strategy is adopted to calculate the average stomatal conductance.

2.3. Material and Design for the Simulations

2.3.1. Modeling Platform

[25] For this study, we use the original three-layer soil version of the ISBA model [*Noilhan and Mahfouf*, 1996; *Boone et al*., 1999]. ISBA is embedded in the *Surface Externalisée* (SURFEX) modeling platform [*Martin et al*., 2007; *Le Moigne*, 2009] of Météo-France. This version of the ISBA model is used together with its upgraded carbon flux version, ISBA-A-gs. In the ISBA-A-gs model, 12 patches are considered in order to represent generic surface types, such as various forest types, grasslands, crops, and bare soil. Most of the ISBA-A-gs parameters are assigned at the patch level. The aggregation of the subgrid model simulations is based on the patch fractions derived from the ECOCLIMAP land cover map [*Masson et al*., 2003]. The standard values of ISBA-A-gs parameters for different vegetation types can be found in the literature [*Gibelin et al*., 2006]. The ISBA-A-gs photosynthesis module can be driven by a satellite-derived LAI climatology using ECOCLIMAP lookup tables. The version that uses climatology of LAI is called "AST" as opposed to the "NIT" version, which is able to dynamically simulate LAI. In the modeling experiments performed in this study, initial states are obtained after a spinup period in order to reach the equilibrium state. SURFEX can be used for both operational and research applications in off-line mode [e.g., *Gibelin et al*., 2006] or coupled with an atmospheric model [e.g., *Sarrat et al*., 2009]. In off-line mode, SURFEX can be forced by atmospheric analyses or by local meteorological observations. In this study, the ISBA-A-gs model is used offline, and there is no feedback from the surface to the atmosphere. We consider the version 7.2 of SURFEX. The required atmospheric forcing fields are: air temperature, air-specific humidity, wind speed, atmospheric pressure, liquid and solid precipitation, and incoming direct and diffuse shortwave and longwave radiation. The observed in situ forcing at one local scale station (Hesse in France—temperate deciduous forest), WFGEI data (Freely Accessible Sources of Meteorological Data) at 36 other local stations (21 sites of conifer, 10 sites of deciduous, and 5 sites of tropical forest, see Table 2) and the global atmospheric forcing from Princeton University [*Sheffield et al*., 2006] are used to evaluate the NEW RT model. WFGEI data result from a recent analysis of surface atmospheric variables based on the ECMWF ERA-Interim Reanalysis (*Weedon et al*., 2011; *Weedon et al*., 2010; *Dee et al*., 2011; *Mitchell and Jones*, 2005; *Rudolf et al*., 2011). The impact of using a NEW multilayer canopy model in ISBA-A-gs will be investigated in section 3 through the analysis of the carbon fluxes.

2.3.2. Local Scale Simulations

[26] The RT transmittance functions are here compared with advanced theoretical RT models involved in the RAdiation transfer Model Intercomparison (RAMI) initiative but also with the DART 3D model. The RAMI initiative benchmarks canopy reflectance models under well-controlled experimental conditions [*Widlowski et al*., 2007]. In the RAMI initiative, validated 3D Monte Carlo models constitute reference simulations of radiation fluxes (absorption, reflection, and transmittance). They are used to assess

Table 3. Description of the RAMI Experimental Conditions Called "HOMO03_TURB"

Set of Parameters (RAMI Experiment Called "HOMO03_TURB")	
Solar zenithal angle	20° or 50°
Leaf area index	3 m^2/m^2
Height of the canopy	1 m
Scatter normal distribution	Uniform
Leaf scattering law	Bi-Lambertian
Leaf scatterer reflectance	0.0546
Leaf scatterer transmittance	0.0149
Soil scattering law	Lambertian
Soil reflectance	0.127

the accuracy and limitations of more simplified RT formulations [*Widlowski et al*., 2011]. RAMI offers the possibility to select spectral, structural, and illumination conditions, together with the leaf inclination (erectophile, planophile, or uniform). We opted here for a standard configuration (see Table 3) where a homogeneous turbid uniform canopy is characterized by a constant probability of foliage interception irrespective of the direction of propagation in that medium. The evaluation of the proposed transmittance functions is carried out for the RAMI case study called "HOMO03_TURB." The set of parameters for this experiment is presented in Table 3: the canopy has a LAI of 3, the zenith angle is equal to 20° or 50°, and the leaf orientation is uniform. In addition, the sensitivity to the leaf orientation and the vertical grid resolution is investigated using the DART 3D model. DART is designed for scientific research, in particular related to numerical remote sensing experiments [*Gastellu-Etchegorry et al*., 1996]. It simulates radiative transfer in the Earth-Atmosphere system, for any wavelength in the optical domain (visible, near infrared, and midinfrared). It must be noticed that DART took part of the RAMI experiment like other advanced theoretical RT models. The reliability of the RT transmittance function is also appraised through comparison with the vertical profile of PAR measured by *Baldocchi et al*. [1985] at several levels in the oak-hickory forest located near Oak Ridge, Tennessee. In a second step, in order to evaluate the performance of the NEW vegetation RT scheme in ISBA-A-gs, no less than four photosynthesis light-response studies are carried out, with respect to the number of layers within the canopy, to the diffuse fraction, to the illumination condition (solar zenith angle), and to the canopy density (LAI). Also, the sensitivity to uncertainties in the representation of leaf orientation and clumping index is discussed. In a third step, simulated GPP are compared against measurements at 37 ground stations belonging to the Flux Network (FLUXNET, (http://daac.ornl.gov/FLUXNET/fluxnet.shtml).

2.3.3. Global Simulations

[27] Global modeled FAPAR and GPP are compared to observation-based estimates [*Beer et al*., 2010] and to MODIS satellite-derived estimates. Concerning MODIS, we used the annual product MOD17A3 that includes a cumulative annual composite of GPP values based on the light use efficiency concept. As for FAPAR, the 4 day MYD15A2 product was handled. ISBA-A-gs is forced by the atmospheric variables provided by Princeton University at 1° resolution at global scale for the year 2006. The seasonal cycle of LAI is provided by ECOCLIMAP-II. This set of simulations will be referred as "AST" in the remaining. The same simulations are then performed with a time-evolving LAI, derived directly from ISBA-A-gs simulations of carbon exchanges. These simulations will be referred to as "NIT," which stands for nitrogen dilution–based representation of leaf biomass in addition to the "AST" capability. The same

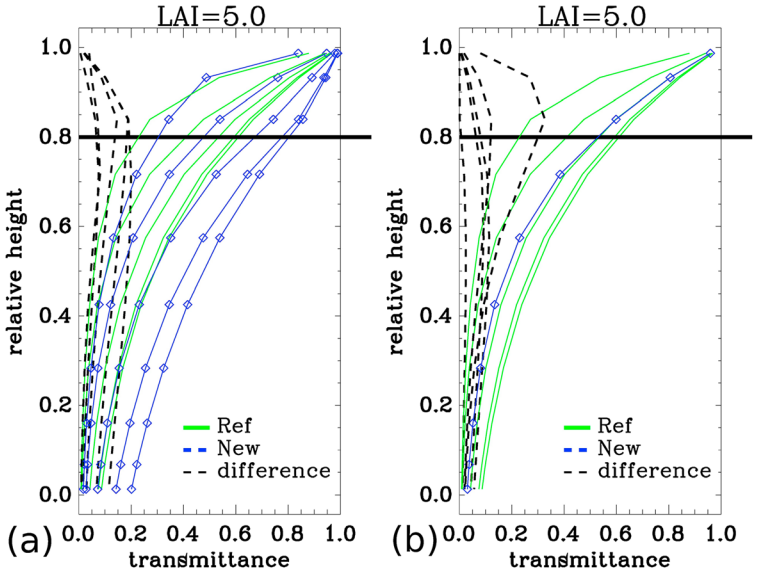

Figure 1. Vertical profile of the transmittance function for a canopy with LAI = 5 for various values of the solar zenith angle (from right to left 0°, 20°, 40°, 60°, and 80°) in case of a (a) direct illumination or (b) diffuse illumination. In blue color: NEW. In green color: REF. In black color: the absolute difference between NEW and REF ("difference"). Transmittance monotonically decreases with the zenith angle except with NEW for the diffuse case (Figure 1b).

Table 4. Comparison of FAPAR and Transmittance Quantities Between RAMI Models for a Homogeneous Turbid Uniform Canopy and the NEW Radiative Transfer Model in ISBA-A-gs

	Solar Zenithal Angle			
	20°		50°	
Model	RAMI	ISBA-A-gs	RAMI	ISBA-A-gs
FAPAR	0.80	0.72	0.89	0.82
Transmittance	0.21	0.26	0.10	0.14

representation of biophysical processes is used in "AST" and "NIT" simulations, except for constrained (from ECOCLIMAP) and unconstrained LAI.

3. Results

3.1. Evaluation of the Vegetation Transmittance Functions

[28] The values of transmittance for different levels through the canopy under different angular conditions of illumination are displayed in Figure 1a. A sigmoid-like shape is noticeable at large values of the solar zenith angle, as it could be expected. In this example, the incident beam impinging the top of the canopy is assumed to be direct, and LAI is fixed at a large value of 5 in order to display a large range of LAI distribution. In comparison, the attenuated beam in diffuse conditions ($fd_{sky} = 1$) is sizable except for high solar zenith angles (see Figure 1b). Transmittance functions in the original version of ISBA-A-gs [*Calvet et al*., 1998] are plotted in green (Figures 1a and 1b).

[29] The dependability of NEW is now verified through a comparison with the RAMI advanced theoretical models of radiative transfer. Table 4 presents these results of comparison between RAMI and the NEW RT model for the fields of FAPAR and transmittance. These radiative quantities simulated by NEW do not match completely the results of RAMI experiments. For example, the RAMI FAPAR for the considered homogeneous turbid medium is 0.80 for a zenithal angle of 20° against 0.72 derived from NEW. The accuracy assessment of our model, with respect to RAMI, could probably be improved by optimizing the set of parameters. However, the overall objective here is to verify the adequacy of the model for further use at global scale when the properties of the canopy (geometry, structure) must be determined somewhat arbitrarily. Moreover, this comparison exercise is solely realized with a direct illumination of the canopy, whereas in practice, the diffuse atmospheric component should be accounted for. In this regard, it was noticed that the RAMI model-to-model agreements generally deteriorate as the plant canopies switch toward a more complex structure, with largest biases observed for canopy absorption and transmission simulations dealing with diffuse illumination conditions [*Widlowski et al*., 2011]. Moreover, *Knyazikhin et al*. [2005] have shown that the radiation penetrating through the lateral sides of the canopy is influenced by the neighboring environment, especially on cloudy days. For example, a transmittance of 0.05 measured at the soil background level for a forest stand surrounded by an optically black lateral boundary could turn to 0.4 if this same forest is now isolated and receives solar light through a cloud filter. However, in practice, such illumination effects are clearly difficult to be accounted for with a high level of precision.

[30] Also, a measurement of the impact of the leaf inclination on the transmittance is sought here with the use of DART 3D RT model. For such, the "HOMO03_TURB" experiment presented during the RAMI exercise with LAI = 3 for a canopy lit by a solar zenithal angle of 20° has been reproduced from the DART model for vertical, uniform, planophile, erectophile, horizontal, and ellipsoidal leaf orientations, giving respective transmittance values of 0.53, 0.24, 0.32, 0.54, 0.07, and 0.42. We consider the first 10 vegetation layers for DART. The obtained transmittance values with NEW for a uniform leaf orientation is equal to 0.26 against 0.24 here below with DART with a 10-layer configuration. Considering now 100 layers, the DART simulations give a value of 0.21 for the total canopy transmittance as already found with the RAMI initiative for the same numerical experiment. This simple exercise shows that 10 layers in the canopy are likely not sufficient if high accuracy is searched on the transmittance factors. The sensitivity of DART to the grid size resolution is illustrated in Figure 2 for the configuration test described in Table 3. The accuracy decreases if the grid sharpness is reduced or if the solar zenithal angle amplifies. Hence, it can be affirmed that at least 10 layers seems to be required in the model if an accuracy threshold of 25% is targeted.

[31] In order to complete the evaluation of the RT transmittance function, a comparison between measured and modeled vertical profiles of PAR in the oak-hickory forest of Oak Ridge is performed at several levels within the canopy at a fully leafed period (30 September 1981). The following forest properties measured by *Baldocchi et al*. [1985] are used

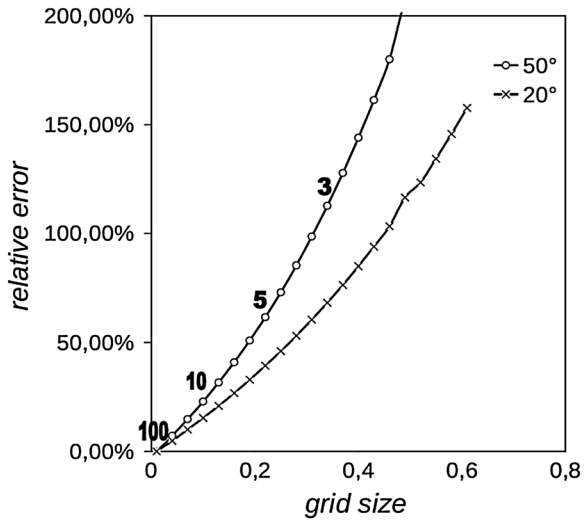

Figure 2. Relative error of the vegetation transmittance estimation given by the DART radiative transfer model versus its vertical grid size in meter for two solar zenith angles [20°, 50°]. The vegetation properties are defined according to RAMI experiment "HOMO03_TURB" (see Table 2). A turbid uniform medium of 1 m height is considered with a LAI = 3. The number of layers within the medium varies from 100 to 2 with 100, 10, 5, and 3 indicated on the upper curve.

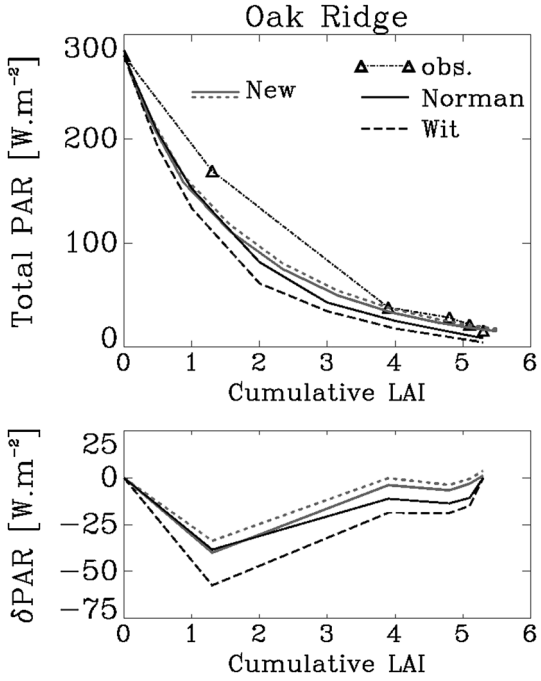

Figure 3. (top) Comparison of calculated and measured mean daily vertical profiles of PAR function of the cumulative LAI in the broadleaf forest of Oak Ridge in Tennessee, 30 September 1981: measured by *Baldocchi et al*. [1985] (black dashed line with triangles), computed with the models of Norman (black line) and de Wit (black dashed line) given by *Baldocchi et al*. [1985], and modelled with NEW using observed leaf orientations (grey line) and a constant g=0.5 (grey dashed line). (bottom) The corresponding differences (δPAR = modeled-measured).

as inputs to our RT scheme: LAI, leaf orientation below and above the crown closure at different hours, transmissivity, reflectivity, and scattering coefficient of Quercus alba and forest floor in the PAR domain and atmospheric conditions (solar elevation, incident PAR). Mean daily vertical profiles of simulated and measured total PAR are reported in Figure 3. Vertical profiles of PAR computed by *Baldocchi et al*. [1985] for the models of *Norman* [1979] and *de Wit et al*. [1965] are also superimposed. Following the example of these later two models, our RT model underestimates values of transmitted PAR in the upper canopy by about 40 W m^{-2}. In the lower canopy, our RT model shows a reasonable comparison with in situ measurements, while the two other models both slightly underestimate the measured values by 10–20 W m^{-2}. The measured variations of the leaf orientation function, g, along the day is introduced in the results of Figure 3 which also displays for the sake of comparison the constant value of $g = 0.5$ adopted by default in our RT model. In fact, the collected data sets indicate canopy layers to be more erectophile in the upper levels (crown domain) than in the lower levels, i.e., $g = 0.61$ against $g = 0.57$, respectively, in terms of daily means. Indeed, g may vary during the day [*Baldocchi et al*., 1985, Table 2]. However, *Baldocchi et al*. [1984] also showed that the leaf orientation distribution exhibits a nonlinear evolution with depth, departing from mostly planophile in the bottom canopy strata (more than 50% of the leaves are inclined at an angle less than 10°), to more erectophile in the top canopy strata, with leaf inclination up to 70°. In this case, using our generic parameterization of the vertical PAR interception tends to underestimate the measurements, as it is clearly not designed to capture such detailed variations.

3.2. Canopy Light-Response Curves

[32] A sensitivity study of the RT model is conducted here. The atmospheric forcing from 2001 to 2007 in the deciduous broadleaf forest of Hesse located in northeastern France [*Granier et al*., 2008] is used. The ISBA-A-gs model is driven by the imposed values of LAI (see section 2.3).

3.2.1. Sensitivity to the Number of Layers

[33] The sensitivity to the number of layers within the canopy is diagnosed here with the GPP field. The GPP is plotted as a function of the incident PAR for a canopy having LAI = 1 (see Figure 4). The dependence of GPP on temperature is avoided by limiting the variations of leaf temperature between 20°C and 25°C. We also place a disregard to shading effects. Again, it appears that at least 10 levels are necessary to minimize the dependence of the radiative transfer scheme on the number of layers. In the remaining, 10 levels within the canopy will be considered. Also, the impact of the diffuse radiation on the produced photosynthesis was investigated with results mirrored in Figure 4. Direct light appears to be less efficient than diffuse light for photosynthesis, as expected. This finding is in agreement with the

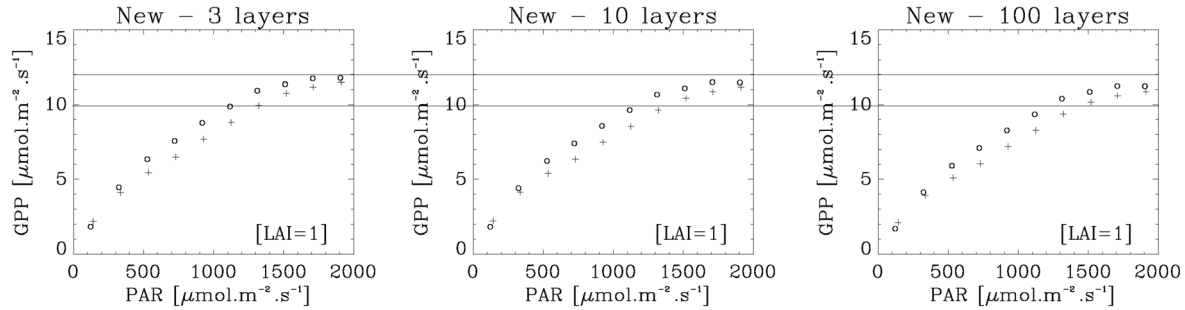

Figure 4. ISBA-A-gs-modeled light response of the GPP of a broadleaf forest to direct PAR (crosses) and diffuse PAR (circles) for NEW with LAI = 1 and sliced in different layers (3, 10, and 100 levels) with a disregard to shading. GPP dependence on temperature is avoided by limiting the leaf temperature between 20°C and 25°C.

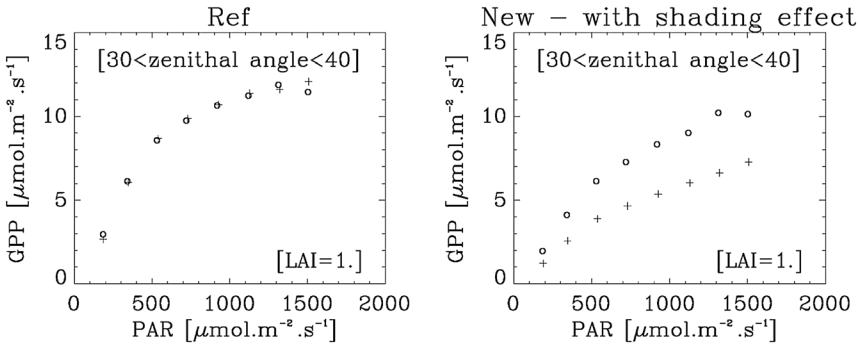

Figure 5. Light response of the GPP of a broadleaf forest to direct PAR (crosses) and diffuse PAR (circles) modeled by ISBA-A-gs with REF and NEW. LAI is fixed to 1. In contrast to Figure 4, sunlit and shaded leaves are accounted for. The GPP dependence on temperature and on solar zenith angle is avoided by limiting the leaf temperature between 20°C and 25°C and the solar zenith angle between 30° and 40°.

aforementioned sensitivity study conducted with the DART radiative transfer model (see section 3.1).

3.2.2. Sensitivity to the Diffuse Fraction

[34] In this sensitivity test, LAI at the Hesse station is fixed to 1, and only GPP values produced by leaves having a temperature between 20°C and 25°C are retained in order to avoid temperature dependence. Because diffuse effects are more critical for relatively high solar zenith angles (see next sensitivity study), only GPP values obtained at solar zenith angles between 30° and 40° are considered. While the GPP light responses to direct and diffuse PAR are similar with REF, the two curves largely differ for NEW (see Figure 5). For example, for an incident PAR of 500 μmol m^{-2} s^{-1}, REF indicates a GPP close to 9 μmol m^{-2} s^{-1} for both direct and diffuse incident solar beams. In contrast, NEW indicates GPP values around 4 μmol m^{-2} s^{-1} for a direct beam and 7 μmol m^{-2} s^{-1} for a diffuse beam.

3.2.3. Sensitivity to LAI

[35] Another interesting point is the response of the net assimilation of a leaf representing the average characteristics of the whole canopy to LAI. Here we conduct a sensitivity analysis on LAI in order to check the relationship between averaged canopy net assimilation and LAI. In this sensitivity analysis, contrary to the other simulations, the soil water content has no impact on photosynthesis (the moisture stress function applied to stomatal conductance is not activated). The LAI is fixed at constant values ranging from 0.3 to 7.0 during the 7 year period (a linear increase

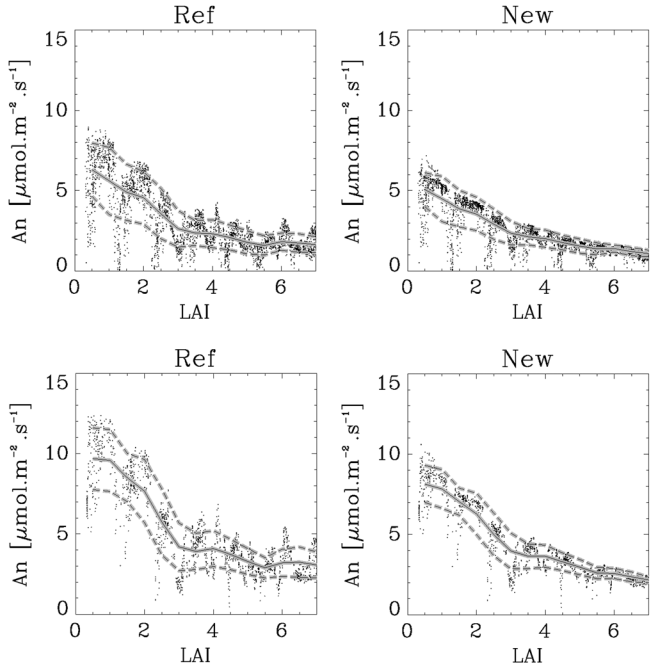

Figure 6. Dependence of leaf net assimilation (An) on LAI as simulated by ISBA-A-gs using (left) REF and (right) NEW. Only direct radiation having an incident PAR value around (top) 100 W/m^2 and (bottom) 200 W/m^2 are used. Solid and dashed gray lines represent the average and the standard deviation of the An values obtained for a given LAI.

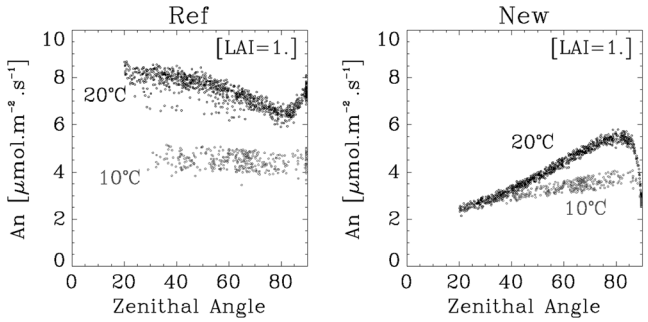

Figure 7. Leaf net assimilation (An) of a broadleaf deciduous forest simulated by (left) REF and (right) NEW, as a function of the solar zenith angle for two-leaf temperature (10°C in gray and 20°C in black). LAI is fixed to 1. Atmospheric diffuse fraction is set to zero. Only direct radiation having an incident PAR value around 100 W/m^2 is used.

from 1 January 2001 to 31 December 2007). The dependence study is performed for two PAR values of 100 and 200 W/m^2. This experiment shows that the mean leaf A_n decreases when LAI increases due to a multiplication of independent leaves while maintaining fixed an incoming radiation (Figure 6). The shape of this dependence is similar to the findings of *Bonan et al*. [2012]. An interesting outcome is the decrease of the dispersion of GPP values obtained for a given LAI with NEW. The GPP standard deviation is reduced by around 30% for low LAI values and by 50% for LAI values beyond 5 (Figure 6). It seems that the GPP simulation is more constrained by the incident PAR with NEW than with REF. This feature will be confirmed further below.

3.2.4. Dependence on Solar Zenith Angle

[36] In order to highlight the dependence of An on the solar geometry, the ISBA-A-gs model is used in a configuration avoiding all effects except anisotropy of illumination. Also, LAI is fixed to 1, stress functions are not activated, and finally only An values produced by leaves having a temperature around 20°C and 10°C are considered. The diffuse fraction is forced to be zero at the top of the canopy (direct beam only), and the incident PAR has a value of 100 W/m^2. The dependence of photosynthesis on solar zenith angle is presented in Figure 7. The leaf level assimilation is enhanced early in the morning or late in the evening compared to noontime if the NEW radiative transfer within the canopy is activated. Photosynthesis is more efficient at large solar zenith angles. The opposite behavior is observed with REF. Since the intercepted solar radiation should be the largest at low zenithal angles (early in the morning or late in the evening), the solar zenith angle impacts photosynthesis in a more realistic way with NEW than with REF. Moreover, the original dispersion of modeled GPP that can be due to a marked dependence on leaf temperature is reduced with NEW. This reduced dependency on leaf temperature appears to be linked to the additional radiative constraint, resulting from the use of NEW (see previous section).

3.2.5. Sensitivity to Leaf Orientation and Clumping Index (Ω)

[37] The geometry of the canopy is well summarized by the leaf inclination angle distribution. However, environmental conditions may lead to tilted leaves in case of heavy rain or bent leaves during heat waves. These stress factors also generally lead to transform a random canopy into a more clumped canopy with the adoption of several levels of aggregation. To anticipate such possible effects, simulations of the PAR flux inside the canopy are here performed for different leaf orientation values (g—function values between 0 and 1) and values of zenithal angles of 30° and 60°. Figure 8 shows that the relative error on FAPAR due to the uncertainty on leaf orientation reaches a maximum at the top of the canopy. Then, the error decreases rapidly with increasing canopy depth because the diffuse component is multidirectional. The phenomenon is more acute for higher values of the solar zenith angle (Figure 8). Note that CLM uses the weak planophile assumption for temperate and boreal broadleaf forests [*Bonan et al*., 2011]. Further, the uncertainty on the clumping index Ω is also shown to have a larger impact in the top layers of the canopy but with less reduction with depth compared to leaf orientation factor (Figure 9).

3.3. GPP Estimates Over Ground Stations

[38] In this section, the impact of the multilayer canopy model on GPP estimations is assessed over dense vegetation areas in comparison with in situ measurements. Two runs of ISBA-A-gs, one with the current version of the model (REF) and one with the new parameterization (NEW), are compared over 37 stations (see Table 2).

[39] Figure 10 and Figure 11 present for the Hesse Forest (France) the GPP time series from 2001 to 2007 and the GPP response to the incident PAR, respectively, for REF and NEW in comparison to ground measurements. Statistical scores (r/bias/rmse) over the entire period are improved (by 2.5%/40.9%/13.9%, respectively) with NEW. The observed GPP increases sharply in a few days in May, at the beginning of the growing season, in relation to budburst. This rapid growing phase is hard to simulate with a radiative photosynthetic model [*Gibelin et al*., 2006]. When the observed LAI goes beyond 5, which means vegetation has reached maturity, the daily GPP response to the incident PAR is better simulated with NEW than REF in comparison to ground measurements (Figure 11). Also,

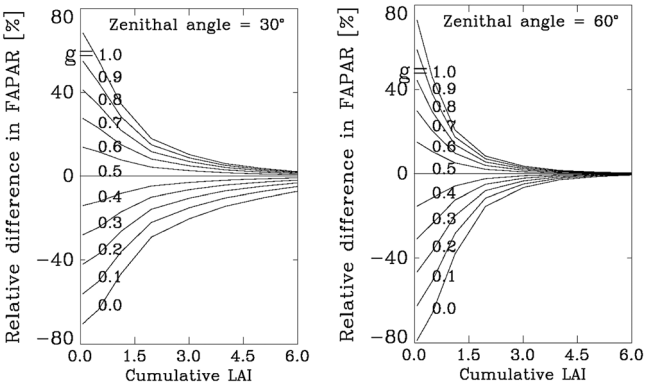

Figure 8. Relative error on FAPAR function of cumulative LAI due to leaf orientation uncertainty. Computation of FAPAR at different level inside the canopy is performed with different leaf orientation values (g function values between 0 and 1) and zenith angle of 30° and 60° (g = 0.5 serves as reference).

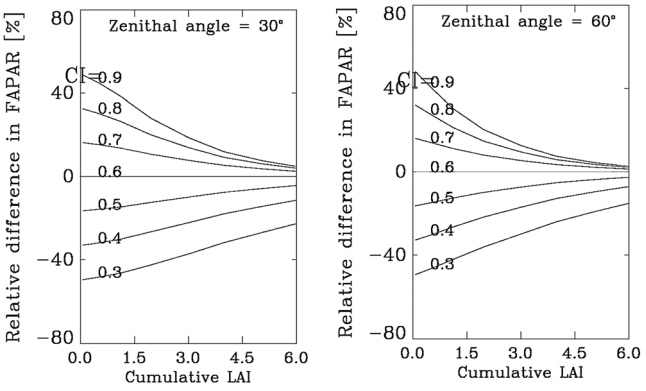

Figure 9. Relative error on FAPAR function of cumulative LAI due to Clumping Index (CI). Computation of FAPAR at different level inside the canopy is performed with CI values (between 0.3 and 0.9) and zenith angle of 30° and 60° (CI = 0.6 serves as reference).

in agreement with a previous remark (see the above sensitivity study to LAI), the NEW scheme simulates less dispersed values of GPP for a given incident radiation, which is in agreement with ground measurements. Standard deviation bars of simulated GPP are reduced (3.5 µmol m^{-2} s^{-1} compared to 4.3 with REF for a mean observed standard deviation of 3.2 µmol m^{-2} s^{-1}). These findings are also manifest if the mean daily cycle of GPP is examined. A monthly average of GPP for June is presented in Figure 12. June was chosen as it represented a long period of time associated with the absence of stress, while the Hesse forest haf already reached its maturity. In comparison with the observations, NEW better describes the daily course of GPP with a reduction of the standard deviation in comparison with observations.

[40] Figure 13 displays the comparison of statistics between simulated and observed GPP for the two model versions (REF versus NEW), over coniferous, deciduous and tropical forests (see Table 2). The statistics are computed from daily values. Each symbol represents 1 year of data at one site. The NEW scheme shows a consistent but moderate increase in correlation for all sites and years. As canopy photosynthesis is the product of A_n and LAI (section 2.2) and because the seasonal cycle of LAI is constrained in the two sets of simulations (REF and NEW), a large increase in the yearly statistical correlation scores was not expected. The RMSE between model and observations decreases with NEW. Also, the average bias is significantly reduced with NEW, especially over tropical forests (see the circles). Note that discarding data sets for stressed periods of time does not affect drastically the results (not shown).

3.4. Global FAPAR and GPP

[41] FAPAR is a biophysical variable that is directly related to photosynthesis. Figure 14 displays a global map of FAPAR from ISBA-A-gs "AST" simulations and MODIS at summertime. The ISBA-A-gs FAPAR estimates are compared to 4-daily MODIS data. We can notice the overestimation of FAPAR computed by ISBA-A-gs with a bias of 0.17 in winter, and 0.16 in summer in comparison with MODIS (see Table 5).

[42] The present work offers the opportunity to present for the first time an estimation of GPP with ISBA-A-gs at the global scale, herein for the year 2006 (see Table 6). ISBA-A-gs overestimates global annual GPP in comparison to a satellite-based product like MODIS and the observation-based estimate of *Beer et al*. [2010] using eddy covariance flux data and various diagnostic models. The small bias of GPP between MODIS and *Beer et al*. [2010] is in agreement with the findings of *Ryu et al*. [2011]. It is worth mentioning that this GPP overestimation is not an exclusive behavior of ISBA-A-gs. *Bonan et al*. [2011] also outlined similar features in using CLM4. They suggested that updated photosynthesis formulation due to radiative effects (shading effects) reduces

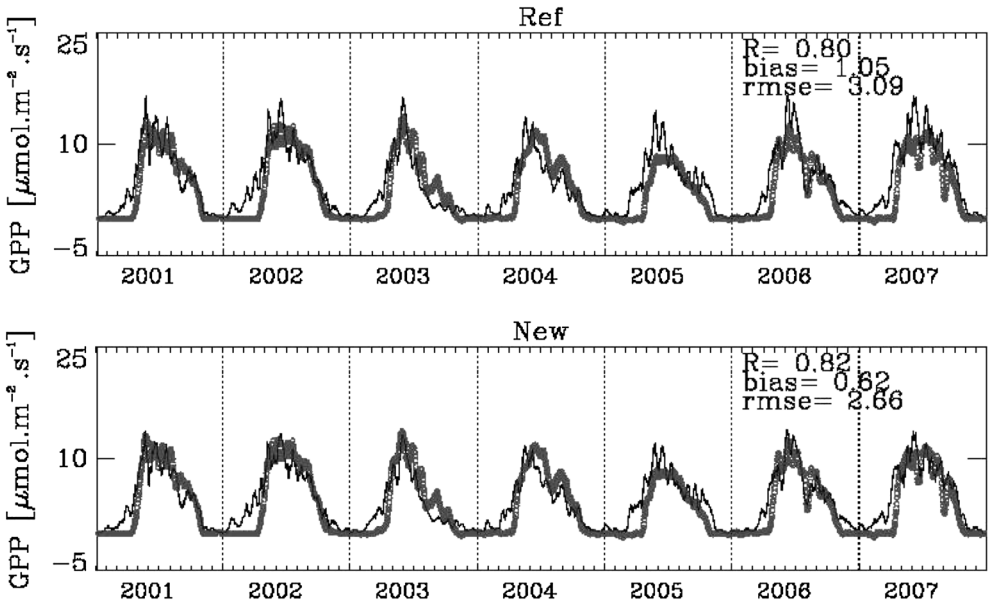

Figure 10. Daily GPP modeled by ISBA-A-gs (dark line) for the Hesse broadleaf forest using REF and NEW. Daily ground measurements of GPP are represented by the gray circles (moving averages, n = 10 days).

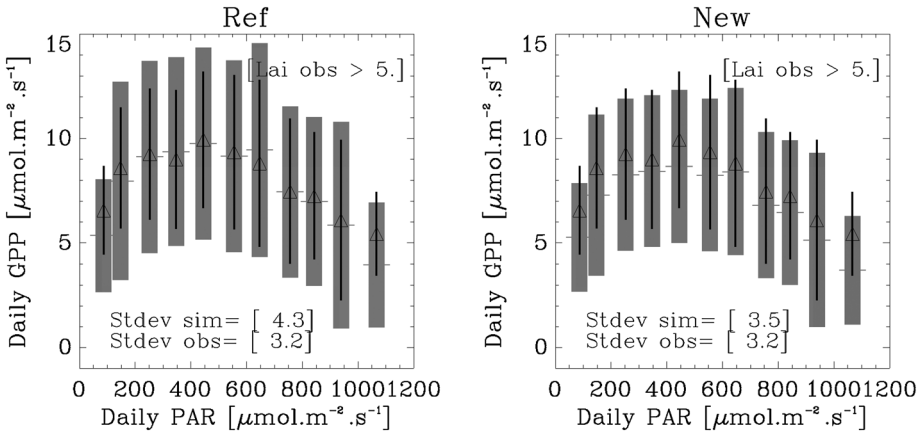

Figure 11. Daily GPP values of the Hesse forest as a function of the incident PAR based on ISBA-A-gs simulations (horizontal tick for mean, grey filled bar for standard deviation) and observations (triangle for mean, black vertical line for standard deviation. Only days having an observed LAI beyond 5 are considered. Standard (stdev) deviations are indicated for both simulations ("sim") and observations ("obs") by bins of 100 μmol quanta per square meter per second.

the 164 PgC yr^{-1} of CLM4 global GPP estimate by 10 PgC yr^{-1}. To obtain a reduction down to 132 PgC yr^{-1}, for instance, an update of the formulation for stomatal conductance is needed, which enhances the impact of the stress factors. Coming back to ISBA-A-gs model, overestimation is decreased by more than 30 PgC yr^{-1} with NEW but the bias is still significant (around 60 PgC yr^{-1}). For REF, the bias is higher with the unconstrained LAI than with the constrained LAI, that is 100 PgC yr^{-1} with NIT against 90 PgC yr^{-1} with AST. With NEW, the biases are about the same values (whatever NIT or AST) and the annual GPP becomes equal to 180 PgC yr^{-1}. Table 6 summarizes these findings and shows a comparison per biome between the modeled GPP and the estimations proposed by *Beer et al*. [2010]. In these latter, tropical forest and savannahs are the most meaningful biomes in terms of global GPP. The ISBA-A-gs estimate for tropical forest is around 60 PgC yr^{-1} for REF against 49 PgC yr^{-1} for NEW. For the sake of comparison, *Beer et al*. [2010] indicate estimates comprised between 40.8 and 43.8 PgC yr^{-1}.

4. Discussion

[43] This study proposed a new canopy RT model aiming at improving the quality of the simulations of carbon flux with ISBA-A-gs for coarse grid scales. However, this upgraded RT model contains a number of underlying assumptions to comply with global applications. The attenuation effect of light due to the presence of woody material is not accounted for. The PAR/Rg ratio is fixed at 0.48, while other values may be found in the literature. For instance, *Baldocchi et al*. [1984] showed that this ratio could decrease from 0.49 above the canopy to 0.27 at the forest floor. Moreover, the canopy is considered as a turbid medium although the option is given here for leafy material to be organized in aggregates through prescribed clumping indices. Besides, we assume the leaves to be randomly oriented and inclined. This offers a simplified vision of the canopy architecture, whereas variations of leaf inclination along the day and depth may be observed [e.g., *Baldocchi et al*., 1984]. Furthermore, with NEW, we attempt to combine the clumping due to gap occurrence in the canopy with the shading effects. The clumping index (Ω) may respond to environmental stress factors (e.g., extreme air temperatures, deficit of light) and could also vary with ancillary factors like LAI dynamic, the fraction of diffuse illumination, and the vegetation type. For these reasons, an accurate assessment of the clumping at the global scale seems to be a difficulty considering the structural differences among covers types that cannot be captured well. *Chen et al*. [2003, 2012] showed that Ω has a significant impact on the global distribution of GPP. They found that the amount of shaded leaves is impacted by the degree of clumping and that shaded leaves contribute up to 35% to the global total GPP, with 50% reported for trees. Indeed, a misunderstanding of the effect of canopy architecture due to Ω could easily result in a

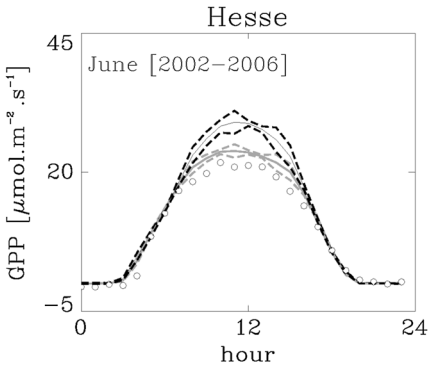

Figure 12. June averaged daily cycle of GPP in Hesse from 2002 to 2006. GPP modeled with ISBA-A-gs REF and NEW are in black and gray, respectively. Solid lines represent the monthly average; dashed lines represent the standard deviation around the mean. Ground measurements of GPP are plotted in grey circle. Statistical scores (bias/rmse) with REF, and NEW are 2.6/0.63, and 1.2/0.43 μmol m^{-2} s^{-1}, respectively.

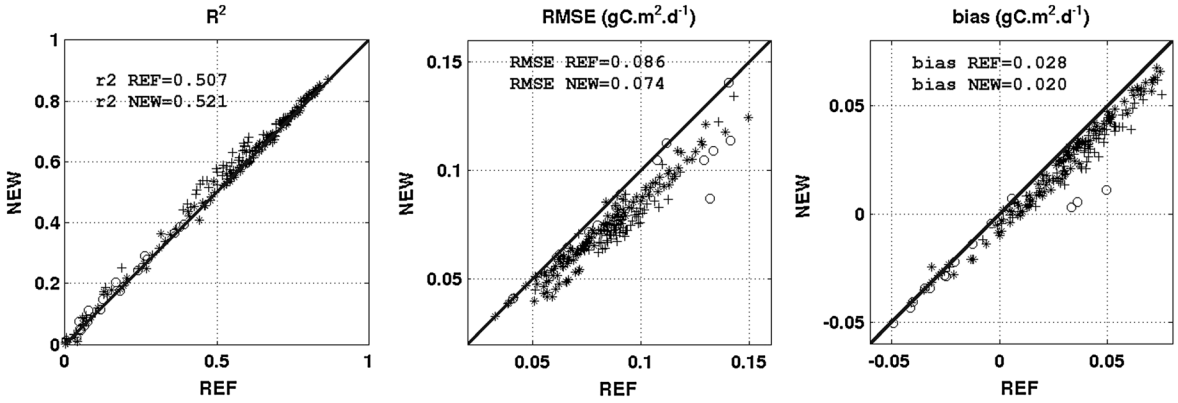

Figure 13. Annual statistical score for a comparison of simulated and observed daily GPP for 36 forested sites (see Table 2). From left to right: correlation, root mean square error, and bias. Each point represents a year for a given station (plus sign, deciduous; asterisk, conifer; open circle tropical).

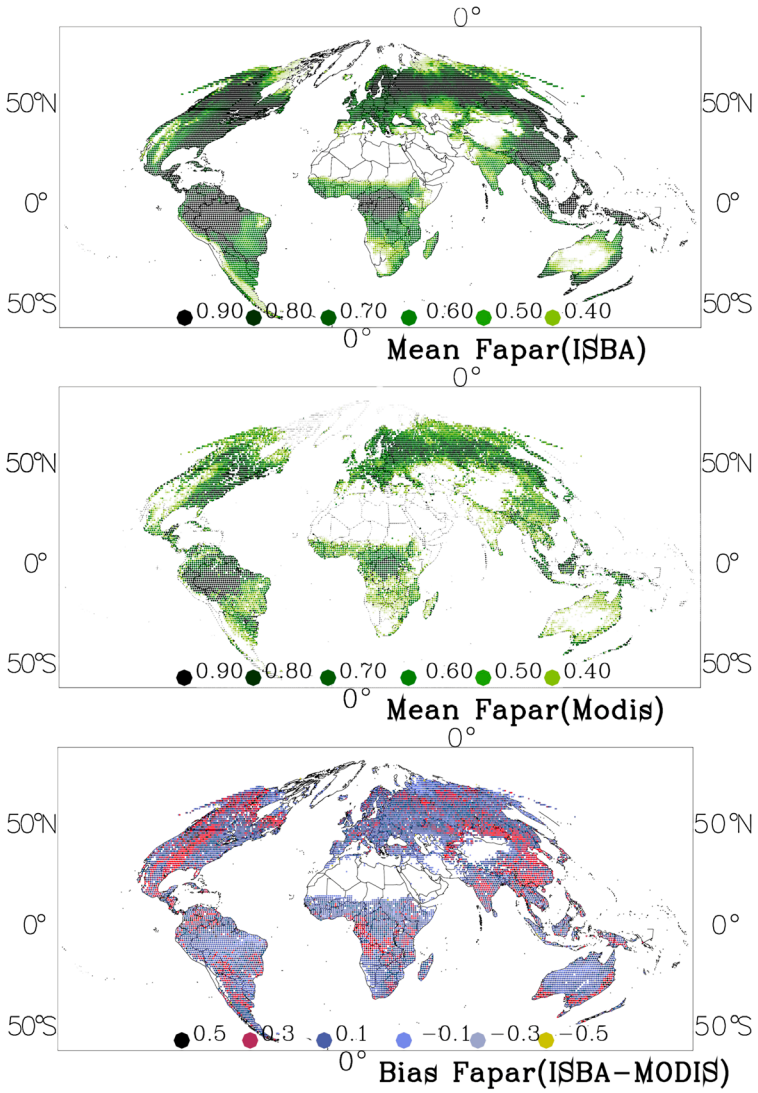

Figure 14. Mean FAPAR at summertime (JJA). From top to bottom: ISBA-A-gs, MODIS (MOD15A3), and difference between the ISBA-A-gs and MODIS estimates.

Table 5. Statistics of Difference (Bias, RMSD, and Temporal Correlation R) Between FAPAR Products From MODIS and ISBA-A-gs ("AST")[a]

		ISBA-A-gs Versus MODIS		
		JFM	JJA	2006
FAPAR	Bias	0.18	0.16	0.17
	RMSD	0.06	0.05	0.04
	R	0.12	0.27	0.51

[a]Estimates are given for winter period (JFM), summer period (JJA), and whole year 2006.

10% error in global GPP estimates. Moreover, the sensitivity tests conducted in this study show that the uncertainties on canopy vertical architecture (leaf orientation or Ω) lead to strong relative error on FAPAR estimations in the upper portion of the canopy. The same conclusion was drawn through a comparison with in situ measurements in the forest of Oak Ridge. These canopy architecture uncertainties within the vertical canopy profile result necessarily in uncertainties on the photosynthesis estimation especially in this upper portion where the light attenuation usually reach its maximum value. In this regard, this work is only a first step toward the representation of an heterogeneous canopy. Overall, not only the canopy vertical architecture should be depicted but also the different vertical atmospheric conditions within the canopy (CO_2 concentration, air temperature humidity, and wind), and the different vertical morphological (area, thickness, and area per mass), biochemical (nitrogen and chlorophyll concentrations), and physiological (ligh-satured photosynthetic rate) attributes. All of them were found to play major roles in the photosynthetic process [*Koike et al*., 2001].

[44] The NEW RT model in ISBA-A-gs tends to decrease the simulated global terrestrial GPP. For 2006, this quantity decreases from 221 to 180 PgC yr^{-1}. This new GPP value is still high with respect to other estimations. Indeed, the GPP values that were reported in the literature range from 107 to 167 PgC yr^{-1} [*Cramer et al*., 2001; *Knorr and Heimann*, 2001]. Various intermediate values were proposed: 123 PgC yr^{-1} [*Beer et al*., 2010], 129 PgC yr^{-1} [*Demarty et al*., 2007], 133 PgC yr^{-1} [*Ruimy et al*., 1996], 109 PgC yr^{-1} [*Zhao et al*., 2005], and 111 PgC yr^{-1} [*Yuan et al*., 2010]. Refining the simulation of water stress conditions or revisiting the parameters of the photosynthesis model could lead to further improvement in the GPP simulations of ISBA-A-gs.

[45] The photosynthesis parameters of ISBA-A-gs are also affected by uncertainties. The recent global database of plant traits [*Kattge et al*., 2011] shows that the specific leaf area ("SLA") parameter, which describes the allocation of leaf area per unit of leaf mass (closely related to canopy leaf nitrogen), presents a large range of values for a given plant functional type (PFT). In contrast, a single value per PFT is used in ISBA-A-gs as it is done in most vegetation models. Another potential source of discrepancy is the lack of an efficient temperature limitation through the mesophyll conductance, and the fact that there is an approximation for the modeled temperature of the leaf due to a single energy budget for both bare soil and vegetation in ISBA. Finally, and as already pointed by *Zhao et al*. [2006], the quality of the atmospheric forcing, could induce notable differences in global GPP estimations, even up and beyond to 20 PgC yr^{-1}.

5. Summary and Conclusion

[46] The use of a new multilayer canopy radiative transfer model (NEW) was investigated in order to obtain better estimates of FAPAR and GPP with ISBA-A-gs. It was shown that at least 10 levels in the canopy are necessary to simulate accurate vegetation transmittance functions. This finding was in agreement with a sensitivity study conducted with the DART radiative transfer model. The canopy light-response curves to the diffuse radiation and to the zenithal angle became more realistic with the use of NEW. The GPP estimation was more constrained by the value of incident PAR with NEW than with REF. The spread of the modeled GPP with NEW was closer to the spread of in situ GPP observations. For example, lower temperature dependence was noticed in relation to the additive radiative constraint resulting from the use of a multicanopy layer model. This result was obtained by thoroughly examining daily cycles of both modeled and in situ GPP. A consequence of these properties triggered by the use of NEW is a reduced sensitivity of the simulations to uncertainties in the incoming radiation.

[47] A proof of concept for LSM simulation of FAPAR was presented. This should find numerous applications in the upcoming years for LSM benchmarking and in the field of assimilation of satellite-derived products. Global mapping of clumping using multiangular satellite data [*Roujean and Lacaze*, 2002; *Chen et al*., 2005] or those of *He et al*. [2012] using MODIS data for 2006 would also certainly be a way to calibrate the coefficients of the RT model and to improve estimations of the modeled FAPAR.

[48] The NEW RT scheme will find an application with a forthcoming upgraded multiple energy version of ISBA-A-gs, in which bare soil and vegetation will be handled separately in terms of both turbulent and radiative fluxes. The

Table 6. GPP for Biomes of the World Estimated by ISBA-A-gs With a Constrained ("AST") or Unconstrained LAI ("NIT"), Observation-Based Estimate by *Beer et al*. [2010], and for MODIS Product

	REF GPP (PgC yr^{-1})		NEW GPP (PgC yr^{-1})			*Beer et al*. [2010] GPP (PgC yr^{-1})
Biome	AST	NIT	AST	NIT	MODIS	
Tropical savannahs and grasslands	56.5	57.9	45.9	42.8		31.3–29.8
Temperate and boreal forests	48.5	47.4	43.5	41.4		18.2–21.4
Tropical forests	60.3	61.4	49.5	49.3		40.8–43.8
Temperate grasslands and shrublands	14.1	14.2	13.6	13.4		8.5–14.0
Other	32.3	40.3	27.7	32.6		22.8–16.2
Total	211.67	221.21	180.16	179.47	114.70	121.7–125.2

use of a multiple-energy budget would affect the leaf temperature response of NEW and would consequently modify the GPP simulations. To move onward, distinguishing estimates of LAI_{sunlit} and LAI_{shade} integrated over the whole vegetation canopy layer could serve to calculate two energy budgets, one for shaded and one for sunlit leaves, and thereby to deliver two temperatures of the vegetation, i.e., $T\text{veg}_{sunlit}$ and $T\text{veg}_{shade}$. Such estimates would permit a better description of temperature dependence of photosynthesis at the canopy level. *Dai et al*. [2004] showed that previous two-stream-big-leaf models developed by *Collatz et al*. [1992], *Sellers et al*. [1992, 1996], *Bonan* [1996], de *Pury and Farquhar* [1997], *Dickinson et al*. [1998], and *Dai et al*. [2003] could be improved in treating separately sunlit and shaded leaves, in terms of radiation absorption and calculation of leaf temperatures, stomatal conductance, and fluxes (water, CO_2, and sensible heat).

[49] Finally, a significant outcome is that the annual global terrestrial GPP simulated by ISBA-A-gs presents a clear overestimation. For 2006, this quantity is comprised between 210 and 221 PgC yr^{-1}, against a value of 123 PgC yr^{-1} given by *Beer et al*. [2010]. The use of NEW decreases this overestimation by 30–40 PgC yr^{-1}, but annual GPP biases remain still sizable at the global scale. *Bonan et al*. [2011] pointed out the same overestimation characteristics with CLM4 and suggested revisiting the parameters of their photosynthesis model. In this perspective, the exhaustive global database of plant traits from TRY [e.g., *Kattge et al*., 2011] would probably be very useful.

[50] **Acknowledgments.** One of us (Sébastien Lafont) was supported by the GEOLAND2 project, which was cofunded by the European Commission within the GMES initiative in FP7. We acknowledge the PI of the in situ measurement (FLUXNET network) made available through the fluxdata.org website. We would like also to thank our colleague Stéphanie Faroux for assisting us in the implementation of these improvements in the SURFEX platform. We are also very grateful to Denis Baldocchi for putting at our disposal the data sets that were acquired at Walker Branch Watershed in Oak Ridge. Finally, fruitful discussions with the NASA/MODIS team and the disposal of the satellite data sets were very appreciated.

References

Baldocchi, D. D., D. R. Matt, B. A. Hutchison, and R. T. McMillen (1984), Solar radiation within an oak-hickory forest: An evaluation of the extinction coefficients for several radiation components during fully-leafed and leafless periods, *Agric. For. Meteorol.*, *32*, 307–322.

Baldocchi, D. D., B. A. Hutchison, D. R. Matt, and R. T. McMillen (1985), Canopy radiative transfer models for spherical and known leaf inclination angle distributions: A test in an oak-hickory forest, *J. Appl. Ecol.*, *22*, 539–555.

Beer, C., et al. (2010), Terrestrial gross carbon dioxide uptake: Global distribution and co-variation with climate, *Science*, *329*(5993): 834–838, doi:10.1126/science.1184984.

Bonan, G. B. (1996), A land surface model (LSM version 1.0) for ecological, hydrological, and atmospheric studies: Technical description and user's guide, *NCAR Tech. Note, NCAR/TN-417ISTR*, 150 pp., Natl. Cent. for Atmos. Res., Boulder, Colo.

Bonan, G. B., P. J. Lawrence, K. W. Oleson, S. Levis, M. Jung, M. Reichstein, D. M. Lawrence, and S. C. Swenson (2011), Improving canopy processes in the Community Land Model version 4 (CLM4) using global flux fields empirically inferred from FLUXNET data, *J. Geophys. Res.*, *116*, G02014, doi:10.1029/2010JG001593.

Bonan, G., K. Oleson, R. Fisher, G. Lasslop, and M. Reichstein (2012), Reconciling leaf physiological traits and canopy flux data: Use of the TRY and FLUXNET databases in the Community Land Model version 4, *J. Geophys. Res.*, *117*, G02026, doi:10.1029/2011JG001913.

Boone, A., J.-C. Calvet, and J. Noilhan (1999), Inclusion of a third soil layer in a land surface scheme using the force-restore method, *J. Appl. Meteorol.*, *38*, 1611–1630.

Bunnik, N. J. J. (1978), The multispectral reflectance of shortwave radiation of agricultural crops in relation with their morphological and optical properties, *Meded. Landbouwhogesch. Wageningen*, 175 pp.

Calvet, J.-C., J. Noilhan, J.-L. Roujean, P. Bessemoulin, M. Cabelguenne, A. Olioso, and J.-P. Wigneron (1998), An interactive vegetation SVAT model tested against data from six contrasting sites, *Agric. For. Meteorol.*, *92*, 73–95.

Calvet, J.-C., A.-L. Gibelin, E. Martin, P. Le Moigne, H. Douville, and J. Noilhan (2008), Past and future scenarios of the effect of carbon dioxide on plant growth and transpiration for three vegetation types of southwestern France, *Atmos. Chem. Phys.*, *8*, 397–406.

Ceulemans, R., and M. Mousseau (1994), Effect of elevated atmospheric CO_2 on woody plants, *New Phytol.*, *127*, 425–446.

Chen, J. M., J. Liu, S. G. Leblanc, R. Lacaze, and J.-L. Roujean (2003), Multi-angular optical remote sensing for assessing vegetation structure and carbon absorption, *Remote Sens. Environ.*, *84*, 516–525.

Chen, J. M., C. H. Menges, and S. G. Leblanc (2005), Global mapping of foliage clumping index using multi-angular satellite data, *Remote Sens. Environ.*, *97*, 447–457.

Chen, J. M., G. Mo, J. Pisek, J. Liu, F. Deng, M. Ishizawa, and D. Chan (2012), Effects of foliage clumping on the estimation of global terrestrial gross primary productivity, *Global Biogeochem. Cycles*, *26*, GB1019, doi:10.1029/2010GB003996.

Collatz, G. J., M. Ribas-Carbo, and J. A. Berry (1992), Coupled photosynthesis—stomatal conductance model for leaves of C4 plants, *Aust. J. Plant Physiol.*, *19*, 519–538.

Cramer, W., et al. (2001), Global response of terrestrial ecosystem structure and function to CO2 and climate change: Results from six dynamic global vegetation models, *Global Change Biol.*, *7*(4), 357–373, doi:10.1046/j.1365-2486.2001.00383.x.

Dai, Y., et al. (2003), The Common Land Model (CLM), *Bull. Am. Meteorol. Soc.*, *84*, 1013–1023.

Dai, Y., R. E. Dickinson, and Y.-P. Wang (2004), A two-big-leaf model for canopy temperature, photosynthesis, and stomatal conductance, *J. Clim.*, *17*, 2281–2299.

Dee, D. P., et al. (2011), The ERA-Interim reanalysis: Configuration and performance of the data assimilation system, *Q. J. R. Meteorol. Soc.*, *137*, 553–597.

de Pury, D. G. G., and G. D. Farquhar (1997), Simple scaling of photosynthesis from leaves to canopy without the errors of bigleaf models, *Plant Cell Environ.*, *20*, 537–557.

Demarty, J., F. Chevallier, A. D. Friend, N. Viovy, S. Piao, and P. Ciais (2007), Assimilation of global MODIS leaf area index retrievals within a terrestrial biosphere model, *Geophys. Res. Lett.*, *34*, L15402, doi:10.1029/2007GL030014.

DeWit, C. T. (1965), Photosynthesis of leaf canopies, *Agric. Res. Rep., 663*, Cent. for Agric. Publ. and Doc., Wageningen, Netherlands.

Dickinson, R. E., M. Shaikh, R. Bryant, and L. Graumlich (1998), Interactive canopies for a climate model, *J. Clim.*, *11*, 2823–2836.

Dufrêne, E., H. Davi, C. François, G. le Maire, V. Le Dantec, and A. Granier (2005), Modelling carbon and water cycles in a Beech forest. Part I: Model description and uncertainty analysis on modeled NEE, *Ecol. Model.*, *185*, 407–436.

Duncan, W. G., R. S. Loomis, W. A. Williams, and R. Hanau (1967), A model for simulating photosynthesis in plant communities, *Hilgardia 38*(4), 181–205.

Duthoît, S., V. Demarez, J.-P. Gastellu-Etchegorry, E. Martin, and J.-L. Roujean (2008), Assessing the effects of the clumping phenomenon on BRDF and FAPAR of a maize crop based on 3D numerical scenes using DART code, *Agric. For. Meteorol.*, *148*, 1341–1351.

Erbs, D. G., S. A. Klein, and J. A. Duffie (1982), Estimation of the diffuse radiation fraction for hourly, daily and monthly average global radiation, *Sol. Energy*, *28*, 293–302.

Fitter, A. H., and R. K. M. Hay (2002), *Environmental Physiology of Plants*, 3rd ed., Academic, Great Britain.

Gastellu-Etchegorry, J. P., V. Demarez, V. Pinel, and F. Zagolski (1996), Modelling radiative transfer in heterogeneous 3-D vegetation canopies, *Remote Sens. Environ.*, *58*, 131–156.

Gibelin, A.-L., J.-C. Calvet, J.-L. Roujean, L. Jarlan, and S. O. Los (2006), Ability of the land surface model ISBA-A-gs to simulate leaf area index at the global scale: Comparison with satellites products, *J. Geophys. Res.*, *111*, D18102, doi:10.1029/2005JD006691.

Goudriaan, J. (1977), *Crop Micrometeorology: A Simulation Study*, Pudoc, Wageningen, Netherlands.

Goudriaan, J. (1986), A simple and fast numerical method for the computation of daily totals of crop photosynthesis, *Agric. For. Meteorol.*, *38*, 249–254.

Goudriaan, J., H. H. van Laar, H. van Keulen, and W. Lovwerse (1985), Photosynthesis, CO_2 and plant production, in *Wheat Growth and Modeling*, *NATO ASI Ser., Ser. A*, vol. *86*, edited by W. Day and R. K. Atkin, Vol. *86*, pp. 107–122, Plenum, New York.

Granier, A., N. Bréda, B. Longdoz, P. Gross, and J. Ngao (2008), Ten years of fluxes and stand growth in a young beech forest at Hesse, North-eastern France, *Ann. Sci.*, *65*, 704, doi:10.1051/forest:2008052.

He, L., J. M. Chen, J. Pisek, C. B. Schaaf, and A. H. Strahler (2012), Global clumping index map derived from the MODIS BRDF product, *Remote Sens. Environ.*, *119*, 118–130, 0034–4257, doi:10.1016/j.rse.2011.12.008.

Houghton, R. A. (1995), Land-use change and the carbon cycle, *Global Change Biol.*, *1*(3), 275–287.

Jacobs, C. M. J. (1994), Direct impact of atmospheric CO2 enrichment on regional transpiration, PhD thesis, Agric. Univ., Wageningen, Netherlands.

Jarvis, P. G. (1976), The interpretation of the variations in leaf water potential and stomatal conductance found in canopies in the field, *Philos. Trans. R. Soc. London, Ser. B*, *273*, 593–610.

Kattge, J., et al. (2011), TRY—A global database of plant traits, *Global Change Biol.*, *17*, 2905–2935, doi:10.1111/j.1365-2486.2011.02451.

Knorr, W., and M. Heimann (2001), Uncertainties in global terrestrial biosphere modeling: 1. A comprehensive sensitivity analysis with a new photosynthesis and energy balance scheme, *Global Biogeochem. Cycles*, *15*(1), 207–225, doi:10.1029/1998GB001059.

Knyazikhin, Y., A. Marshak, and R. B. Myneni (2005), Three-dimensional radiative transfer in vegetation canopies and cloud-vegetation interaction, in *Three-Dimensional Radiative Transfer in the Cloudy Atmosphere*, edited by A. Marshak and A. Davis, pp. 617–652, Springer.

Koike, T., M. Kitao, Y. Maruyama, S. Mori, and T. T. Lei (2001), Leaf morphology and photosynthetic adjustments among deciduous broad-leaved trees within the vertical canopy profile, *Tree Physiol.*, *21*, 951–958.

Kucharik, C., J. M. Normal, and S. T. Gower (1999), Characterization of radiation regimes in nonrandom forest canopies: theory, measurements, and a simplified modeling approach, *Tree Physiol.*, *19*, 695–706.

Lantinga, E. A., M. Nassiri, and M. J. Kropff (1999), Modelling and measuring vertical light absorption within grass-clover mixtures, *Agric. For. Meteorol.*, 71–83.

Laurila, T. (2002), Vaisala News Articles, Retrieved December 2010, from Carbon Cycles of the Ecosystems of the World.

Le Moigne, P. (2009), SURFEX scientific documentation, *Note Cent. Groupe Meteorol. Moyenne Echelle*, *87*, 211 pp., Cent. Natl. de Rech. Météorol., Météo-France, Toulouse, France. [Available at: http://www.cnrm.meteo.fr/surfex/, last access: July 2010), CNRM, Toulouse, 211 pp.

Martin, E., et al. (2007), Le code de surface externalisé SURFEX de Météo-France, paper presented at Ateliers de Mod'elisation de l'Atmosphère, Cent. Natl. de Rech. Météorol., Toulouse, France, 16–18 Jan.

Masson, V., J. L. Champeaux, F. Chauvin, C. Meriguet, and R. Lacaze (2003), A global database of land surface parameters at 1-km resolution in meteorological and climate models, *J. Clim.*, *16*, 1261–1282.

McCree, K. J. (1966), A solarimeter for measuring photosynthetically active radiation, *Agric. Meteorol.*, *3*, 353–366.

Mercado, L. M., N. B. Bellouin, S. Sitch, O. Boucher, C. Huntingford, M. Wild, and P. M. Cox (2009), Impact of changes in diffuse radiation on the global land carbon sink, *Nature*, *458*, 1014–1018.

Mitchell, T. D., and P. D. Jones (2005), An improved method of constructing a database of monthly climate observations and associated high-resolution grids, *Int. J. Climatol.*, *25*, 693–712.

Ni, W., X. Li, C. E. Woodcock, J. L. Roujean, and R. E. Davis (1997), Transmission of solar radiation in boreal conifer forests: Measurements and models, *J. Geophys. Res.*, *102*, 29,555–29,566.

Ni-Meister, W., and H. Gao (2011), Assessing the impacts of vegetation heterogeneity on energy fluxes and snowmelt in boreal forests, *J. Plant Ecol.*, *4*, 37–47.

Noilhan, J., and J. F. Mahfouf (1996), The ISBA land surface parametrisation scheme, *Global Planet. Change*, *13*, 145–159, doi:10.1016/0921-8181(95)00043-7.

Norman, J. M. (1979), Modelling the complete crop canopy, in *Modification of the Aerial Environment of Plants*, edited by B. J. Barfield and J. F. Gerber, Am. Soc. of Agric. Eng., St. Joseph, Mich.

Ross, J. (1975). Radiative transfer in plant communities, in *Vegetation and the Atmosphere*, edited by J. L. Monteith, pp. 13–55, Academic, London.

Ross, J. (1981), *The Radiation Regime and Architecture of Plant Stands*, Springer, New York.

Roujean, J.-L. (1996), A tractable physical model of shortwave radiation interception by vegetative canopies, *J. Geophys. Res.*, *101*(D5), 9523–9532.

Roujean, J.-L. (1999), Measurements of PAR transmittance within boreal forest stands during BOREAS, *Agric. For. Meteorol.*, *93*, 1–6.

Roujean, J.-L., and R. Lacaze (2002), Global mapping of vegetation parameters from POLDER multiangular measurements for studies of surface-atmosphere interactions: A pragmatic method and its validation, *J. Geophys. Res.*, *107*(D12), 4150, doi:10.1029/2001JD000751.

Rudolf, B., et al. (2011), New GPCC Full Data Reanalysis version 5 provides high quality gridded monthly precipitation data, *GEWEX News*, *21*(2), 4–5.

Ruimy, A., G. Dedieu, and B. Saugier (1996), TURC: A diagnostic model of continental gross primary productivity and net primary productivity, *Global Biogeochem. Cycles*, *10*(2), 269–285, doi:10.1029/96GB00349.

Ryu, Y., et al. (2011), Integration of MODIS land and atmosphere products with a coupled-process model to estimate gross primary productivity and evapotranspiration from 1 km to global scales, *Global Biogeochem. Cycles*, *25*, GB4017, doi:10.1029/2011GB004053.

Sarrat, C., et al. (2009), Mesoscale modelling of the CO2 interactions between the surface and the atmosphere applied to the April 2007 CERES field experiment, *Biogeosciences*, *6*, 633–646.

Schlesinger, W. H. (1997), *Biogeochemistry: An Analysis of Global Change*, Academic Press, San Diego, California, paperback ISBN 0-12-625155-X.

Sellers, P. J., J. A. Berry, G. J. Collatz, C. B. Field, and F. G. Hall (1992), Canopy reflectance, photosynthesis, and transpiration. III. A reanalysis using improved leaf models and a new canopy integration scheme, *Remote Sens. Environ.*, *42*, 187–216.

Sellers, P. J., D. A. Randall, G. J. Collatz, J. A. Berry, C. B. Field, D. A. Dazlich, C. Zhang, G. D. Collelo, and L. Bounoua (1996), A revised land surface parameterization (SiB2) for atmospheric GCMs. Part I: Model formulation, *J. Clim.*, *9*(4), 676–705.

Sheffield, J., G. Goteti, and E. F. Wood (2006), Development of a 50-year high-resolution global data set of meteorological forcings for land surface modeling, *J. Clim.*, *19*, 3088–3111.

Stigter, C. J., and V. M. M. Musabilha (1982), The conservative ratio of photosynthetically active to total radiation in the tropics, *J. Appl. Ecol.*, *19*, 853–858.

Tsubo, M., and S. Walker (2005), Relationships between photosynthetically active radiation and clearness index at Bloemfontein, South Africa, *Theor. Appl. Climatol.*, *80*, 17–25.

Weedon, G. P., S. Gomes, P. Viterbo, H. Österle, J. C. Adam, N. Bellouin, O. Boucher, and M. Best (2010), The WATCH forcing data 1958–2001: A meteorological forcing dataset for land surface and hydrological models. *WATCH Tech. Rep., 22*, 41 pp., Centre for Ecology & Hydrology, UK, [Available at http://www.eu-watch.org/locations].

Weedon, G. P., S. Gomes, P. Viterbo, W. J. Shuttleworth, E. Blyth, H. Österle, J. C. Adam, N. Bellouin, O. Boucher, and M. Best (2011), Creation of the WATCH forcing data and its use to assess global and regional reference crop evaporation over land during the twentieth century, *J. Hydrometeorol.*, *12*, 823–848, doi:10.1175/2011JHM1369.1.

Widlowski, J.-L., et al. (2007), The third RAdiation transfer Model Intercomparison (RAMI) exercise: Documenting progress in canopy reflectance modelling, *J. Geophys. Res.*, *112*, D09111, doi:10.1029/2006JD007821.

Widlowski, J. L., et al. (2011), RAMI4PILPS: An intercomparison of formulations for the partitioning of solar radiation in land surface models, *J. Geophys. Res.*, *116*, G02019, doi:10.1029/2010JG001511.

Yuan, W. P., et al. (2010), Global estimates of evapotranspiration and gross primary production based on MODIS and global meteorology data, *Remote Sens. Environ.*, *114*(7), 1416–1431, doi:10.1016/j.rse.2010.01.022.

Zhao, M. S., F. A. Heinsch, R. R. Nemani, and S. W. Running (2005), Improvements of the MODIS terrestrial gross and net primary production global data set, *Remote Sens. Environ.*, *95*(2), 164–176, doi:10.1016/j.rse.2004.12.011.

Zhao, M. S., and S. W. Runnings (2006), Sensitivity of moderate resolution imaging spectroradiometer (MODIS) terrestrial primary production to the accuracy of meteorological reanalyses, *J. Geophys. Res.*, *111*, G01002.